Dalton Transactions

A rare 4-fold interpenetrated metal-organic framework constructed from an anionic indium-based node and a cationic dicopper linker

Journal:	*Dalton Transactions*
Manuscript ID	DT-ART-03-2021-000764.R1
Article Type:	Paper
Date Submitted by the Author:	07-Apr-2021
Complete List of Authors:	Pappuru, Sreenath; Technion Israel Institute of Technology, Chemical Engineering Idrees, Karam; Northwestern University, Department of Chemistry Chen, Zhijie; Northwestern University, Department of Chemistry Shpasser, Dina; Technion Israel Institute of Technology, Chemical Engineering Gazit, Oz; Technion Israel Institute of Technology, Chemical Engineering

ARTICLE

A rare 4-fold interpenetrated metal–organic framework constructed from an anionic indium-based node and a cationic dicopper linker

Received 00th January 20xx,
Accepted 00th January 20xx

DOI: 10.1039/x0xx00000x

Sreenath Pappuru,[a] Karam B. Idrees,[b] Zhijie Chen,[b] Dina Shpasser[a] and Oz M. Gazit *[a]

A unique 4-fold interpenetrated metal–organic framework, **TIF-1**, was synthesized by combining anionic indium node with cationic linker. This framework shows a rare type of 4-fold interpenetrated **dia** network, constructed from tessellation of biangular and tetragonal type metal–organic micropores. The porosity of **TIF-1** is moderate due to four-fold interpenetration and charge-balancing anions. The cationic feature of this MOF may give good efficiency for selective small anion exchange or separation. In addition, the thermal stability and moderate CO_2 adsorption property of the complex were studied.

Introduction

Metal-organic frameworks (MOFs) or porous coordination polymers (PCPs) are a class of porous crystalline hybrid materials composed of metal ions/clusters and polytopic organic linkers connected together *via* coordination bonds.[1] High surface area, tunable structure and good thermal/chemical stability have made MOFs promising candidates for a wide range of applications including, but not limited to, gas storage,[2] chemical absorption,[3] gas separation,[4] exchange reactions[5] and heterogeneous catalysis.[6] Furthermore, the flexible nature of MOFs opens up a range of possibilities for tuning their functionality.[1d-1g,7a] For example, Kitagawa group synthesized a flexible cadmium based PCP and systematically examined the gas sorption properties of this PCP towards O_2, Ar and N_2. It was identified that the flexible nature of this material, significantly affected the gate-opening pressure (P_{go}) of O_2, Ar, and N_2. The P_{go} reflects the interplay between the guest molecule adsorption and the ability of the host framework to self-transform, via the gate-opening intermediate process, between a closed to an open pore configuration. In their study, based on volumetric isotherms at 90 K, a sudden increase in the P_{go} of O_2, Ar, and N_2 to 3.9, 40.1, and 55.3 kPa, respectively was observed. Using kinetic analysis this process was shown to be governed by intermolecular interaction forces of the guest molecules.[1h]

However, the flexibility of MOFs could also pose a challenge with respect to maintaining permanent access to the pores in the material. This is especially challenging when the target is the formation of a MOF with large pores. In this context, the synthesis of an interpenetrated MOF structure has been proven to be an effective approach for preserving the porous structure.[7b,c,d,11a] However, in order to form large pores, one must use large organic linkers for MOF synthesis. The large size of the linkers will prompt the dual net catenation as a consequence of the large free spaces in a single network and in-turn also promote the filling of the voids.[8] Despite this reduction in pore volume the framework-framework interactions can stabilize the resulting MOF structure.[9] The level of interpenetration depends on multiple synthetic parameters including temperature,[10a] reactant concentration,[10a] solvent,[10b] modulator,[10c] pH,[10d] and the ligand design[10e]. Hence, controlling this synthetic process become a major challenge.

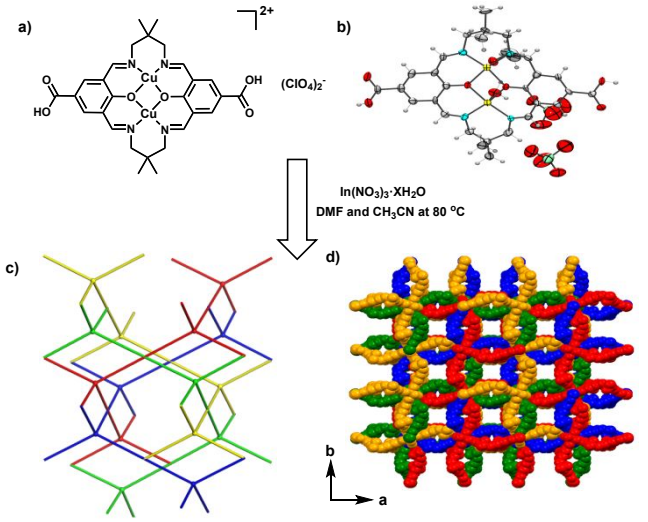

Fig. 1 a) Chemical structure of the dicopper Robson-type ligand, $H_2L^{2+}(ClO_4^-)_2$. [metal coordinated solvents are removed in chemical structure for clarity] b) Crystal structure of ligand $H_2L^{2+}(ClO_4^-)_2$. c) Overall 4-fold interpenetrated unique dia network of **TIF-1** (the four interpenetrating nets coloured red, yellow, green and blue). d) Schematic 3D representation of the crystal structure of **TIF-1** along the *c*-axis

[a] *Faculty of Chemical Engineering, Technion– Israel Institute of Technology, Haifa 320003, Israel.*
[b] *Department of Chemistry, North Western University, 2145 Sheridan Road, Evanston, Illinois 60208, United States.*
† Footnotes relating to the title and/or authors should appear here.
Electronic Supplementary Information (ESI) available: [details of any supplementary information available should be included here]. See DOI: 10.1039/x0xx00000x

Earlier work by Zaworotko and co-workers reported the synthesis of an interpenetrated and a non-interpenetrated primitive cubic (**pcu**) topology in two isomeric Cd(II) mixed-ligand MOFs by controlling synthesis temperature and reactant concentration.[10a] Recently, Hupp's and Farha's group intentionally designed tetraacid organic linkers with aryl-H rather than with the bulkier aryl-Br moieties. Their aim was to use the sterically less demanding aryl-H linkers in order to control the degree of catenation in MOF synthesis. Using this approach, they successfully compiled a library of noncatenated MOFs.[10e] Kitagawa and co-workers reported the control over the degree of interpenetration of a **pcu** network from 2-fold to 3-fold by the use of the solvent molecules as a template.[10b] Serre and co-workers reported the MIL-126 MOF, which is a two-fold interpenetrated version of MIL-88. It was shown that MIL-126 exhibits a higher degree of rigidity and stable porosity compared to flexible non-interpenetrated MIL-88, which undergoes pore collapse.[11] Sun and co-workers managed to construct a 3-fold and 8-fold interpenetrated frameworks using $ThSi_2$ network and a bidentate pyridyl-based ligand of various lengths.[12]

Herein, we describe the synthesis and structure of a charged unique 4-fold interpenetrated MOF (Fig. 1) constructed from a new dicationic Robson-type dicarboxylate linker (Fig. 1a and 1b) and a 4-connected In^{3+} node. Notably, while significant interpenetrated networks based on neutral frameworks have been reported, the charged interpenetrated networks are so far very rare. The unprecedented cationic feature of this MOF may provide good efficiency for selective small anion exchange or separation. As observed previously, the use of an indium node can provide moderate to high stability to the MOF owing to the high valence state and hard acid nature of indium ions (In^{3+}).[13] In the present work the ligand and MOF structures were unambiguously confirmed by single-crystal X-ray diffraction analysis (SCD).

Results and discussion

The dicopper Robson-type ligand $H_2L^{2+}(ClO_4^-)_2$ (Fig. 1a) was synthesized in a single step as shown in Scheme S1 (ESI†), starting from 3,5-diformyl-4-hydroxybenzoic acid, 2,2-dimethyl-1,3-propanediamine and $Cu(ClO_4)_2{\cdot}6H_2O$. Single crystal X-ray diffraction (SCD) measurements of the macrocyclic ligand $H_2L^{2+}(ClO_4^-)_2$ revealed the presence of two five-co-coordinated Cu^{2+} ions with a distorted square pyramidal, which are bound within the macrocyclic Schiff base moiety (Fig. 1b and S2 in ESI†). The corresponding **TIF-1 (**Technion Institute Framework 1) was synthesised through a solvothermal reaction of $H_2L^{2+}(ClO_4^-)_2$ with $In(NO_3)_3{\cdot}xH_2O$ in a mixture of DMF and CH_3CN at 80 °C, forming a green prism-like crystals of $[InL_2]{\cdot}(NO_3)_5{\cdot}x$solvent (Fig. 2a&b). Analysis of the SCD data shows that **TIF-1** crystallized in tetragonal crystal system with *I*-42*d* space group (a = 31.801(17) Å, b = 31.801(17) Å, and c = 31.382(13) Å at 110 K) (Table 1), which is the result of the formation of a pseudosymmetric feature caused by the random orientation and flexibility of the bent type dicopper Robson-type ligand $H_2L^{2+}(ClO_4^-)_2$. The coordination environment of **TIF-1** shows monomeric indium node and each In^{3+} is surrounded by eight oxygen atoms, each from four independent carboxyl groups of the linker. The coordination of the four ligands to each In^{3+} leads to a 4-connected three-dimensional

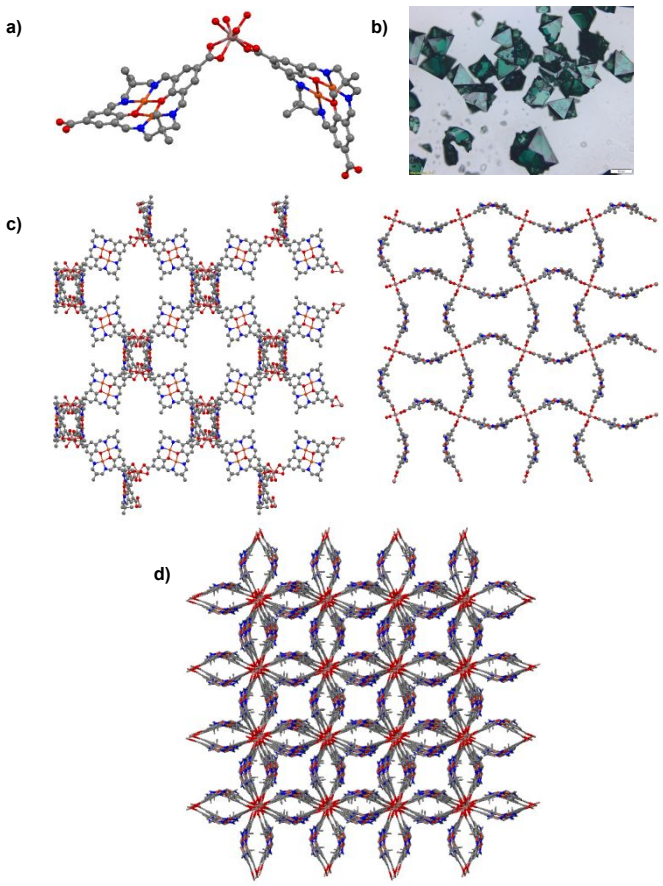

Fig. 2 a) Coordination environment of In^{3+} ion in **TIF-1**. b) Photograph of as-synthesized crystals of **TIF-1**. c) Ball-and-stick view of single 3D network. d) 4-fold interpenetrated 3D network.

3D) framework with interpenetrated **dia** topology.[11c] Topologically, the inorganic indium building unit can be viewed as tetrahedral nodes, linked via ditopic organic ligands to form a 3-peridic **dia** network. This overall structure displays a rare type of 4-fold interpenetrated **dia** net, which is different from the two nets in the Reticular Chemistry Structure Resource (RCSR) database—dia-c4 and dia-c4*.[11b] The crystal parameters, data collection and refinements for $H_2L^{2+}(ClO_4^-)_2$ and **TIF-1** are summarized in Table 1. Notably, the obtained **TIF-1** unusually possess an anionic indium node with cationic linkers. whereas, other recently reported In-MOFs are constructed by a neutral or a cationic indium SBU and a cationic linker.[18,19] Closer inspection of the MOF structure reveals that, the framework is constructed by the tessellation of biangular and tetragonal type metal–organic micropores along the c axis (Fig. 1c, 2d and S3 in ESI †). At each vertex four biangular and four tetragonal type micropores are present labelled as {(2·4)·(2·4)·(2·4)·(2·4)} network (Fig. 2d). Previously, for an indium-based anionic MOF the tessellation of triangular and square metal–organic nanotubes were shown to occur along the a-axis.[19] Herein, the square antiprismatic geometry of the In^{3+} nodes and their link

with the Robson-type ligands lead to a biangular and tetragonal type polygons configuration, which is projected in the *ab* plane (Fig. 2d). As shown in Figure 2c, the analysis of the 3D framework of **TIF-1** reveals that the single 3D network consists of large irregular tetragonal channels (28.6 × 31.5 Å), which are occupied by other independent frameworks, generating the 4-fold interpenetrated charged **dia** network (Fig. 1c, 2d and S3 in ESI†). The phase purity of the bulk material was confirmed by powder X-ray diffraction (PXRD) (Fig. 3a). PXRD measurements of MOF crystals (Fig. 3a) reveals that the pattern closely matches the simulated pattern generated based on the SCD results, indicative of a phase-pure product. PXRD analysis of the **TIF-1** following treatment in various organic solvents showed that the structure does not change (Fig S4). The Fourier transform attenuated total reflection infrared spectroscopy (FTIR-ATR) spectra (Fig. 4) of the **TIF-1** shows a broad band at ca. 3400 cm^{-1} corresponding to the O-H of H_2O and a band at ca. 2900 cm^{-1}–2800 cm^{-1} corresponding to the C-H stretching vibrations of dimethyl-1,3-propanediamine of the ligand.[20] In addition, characteristic bands at ~1639 cm^{-1} corresponding to the C=N of the ligand,[18] the deprotonated carboxylate asymmetric stretching at ca. 1578 cm^{-1} and symmetric stretching at ca. 1316 cm^{-1} were also identified.[2e] The absence of an absorbance band in the range of 1730-1690 cm^{-1} indicates the complete deprotonation of the ligand carboxylic groups.[2e] The band near 1402 cm^{-1} is attributed to the presence of NO_3^- anions, which serve as charge balancing molecules.

Table 1 Crystallographic data for $H_2L^{2+}(ClO_4^-)_2$ and **TIF-1**

Compounds	$H_2L^{2+}(ClO_4^-)_2$	TIF-1
Molecular formula	$C_{30}H_{37}Cu_2N_4O_8,2(ClO_4)$	$C_{56}H_{55}Cu_4$ In N_8O_{12}[S]
Formula weight	907.61	1401.06
T/K	200 K	110 K
Wavelength (Å)	0.71073A	0.71073 A
Crystal system,	Orthorhombic,	Tetragonal,
Space group	$P2_12_12_1$	I-42d
a/ Å	11.982(3)	31.8006(17)
b/ Å	16.944(4)	31.8006(17)
c/ Å	19.081(5)	31.3820(13)
α (°)	90	90
β (°)	90	90
γ (°)	90	90
V/ Å^3	3873.8(18)	31736(4)
Z, Calculated density (g cm^{-3})	4, 1.556	16, 1.173
Absorption coefficient(mm^{-1})	1.310 mm^-1	1.390 mm^-1
ϑ range/°	2.082 to 25.09	1.919 to 25.351
Reflections collected/unique	6873	14471
Independent reflections	2896	3843
Data/restraints/parameters	2896 /0/403	14471/277/738
Goodness-of-fit on F2	1.037	1.018
Final R indices [I >2σ(I)]	R1 = 0.0707, wR2 =0.1825	R1 = 0.0654, wR2 = 0.2081
R indices (all data)	R1 = 0.1014, wR2 = 0.1952	R1 = 0.1396, wR2 = 0.1601
Max. and min. transmission	0.871 and 0.696	0.939 and 0.831
CCDC number	2039820	2039821

$R_1 = \sum|F_0| - |F_c|/\sum|F_0|$, $wR_2 = [\sum (F_0^2 - F_c^2)^2/\sum w(F_0^2)^2]^{1/2}$

The identification of the NO_3^- was difficult to ascertain using only the SCD data, presumably due to the poor diffractions in the SCD as well as disordered nitrate anions in the micropores of the **TIF-1**. To evaluate the oxidation state of the Cu sites, the **TIF-1** was analysed using high resolution X-ray photoelectron spectroscopy (XPS). The binding energies were calibrated to the C1s peak at 284.8 eV (Fig. S5d in ESI†). The results show a peak positioned at a binding energy value of 932.5 eV in the Cu $2p_{3/2}$ region, which corresponds to the Cu(II) state (Fig. S5a in ESI†).[17a] The two satellites bands in the range of 940 to 945 eV further confirm the presence of Cu^{2+} sites. The band 444.6 eV, corresponding to the binding energy of the In3d, shows the In(III) oxidation state (Fig. S5b in ESI†). The bands detected at 406.3 eV in the N1s region confirm the presence of NO_3^- anions (Fig. S5c in ESI†).[17b]

The TGA-MS data of **TIF-1** (Fig. S6 and S7 in ESI †) displays a gradual initial weight loss between 35 and 135 °C, which corresponds to the bulk water (ca. 5% wt, m/z 18). As evident by the TG and MS data, the onset for MOF decomposition starts at ~240 °C, which is consistent with the previous indium MOFs.[18] The CO_2 adsorption isotherm of the **TIF-1** measured at 195 K, showed moderate CO_2 uptake capacity of 30 cm^3/g and has a surface area of ~50 m^2/g (Fig. S8). Following scCO2 activation the PXRD showed a shift in PXRD peaks of **TIF-1**. However, PXRD pattern of the $scCO_2$ activated sample, was validated to be the same as that measured for the sample after physisorption analysis. The low uptake of CO_2 can be attributed to the reduction of pore volume by the interpenetration in addition the presence of charge balancing cations and anions in the pores as well as the flexible nature of **TIF-1**.

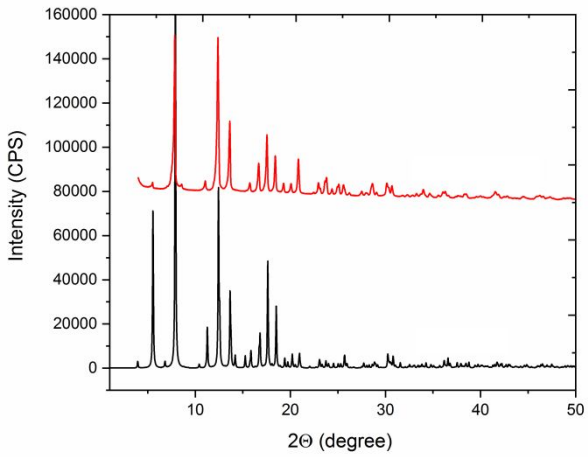

Fig. 3 PXRD pattern simulated from the CIF file of **TIF-1** (black) and PXRD pattern of freshly prepared **TIF-1** (red).

Conclusions

In summary, this work reports the synthesis of a new dicopper Robson-type dicarboxylate flexible ligand and its use for the synthesis of a novel **TIF-1** MOF with 4-fold interpenetrated **dia** net, possessing both anionic nodes and cationic linkers. The linker and MOF both were unambiguously confirmed by single-crystal X-ray diffraction analysis. In contrast with the prolific production of MOFs based on various ligands, the use of

bimetallic Robson-type ligand to construct MOF has only few examples. This work provides access to the synthesis of novel bimetallic core MOF's with advantageous functionality, which lean on the versatile coordination chemistry of the Robson-type ligand. The single-crystal X-ray analysis of the synthesized MOF reveals that, the framework is constructed by the tessellation of biangular and tetragonal type metal–organic micropores along the c axis. It is shown that this 4-fold interpenetrated MOF is highly stable following treatment in various solvents in addition to being stable up to 240 °C. As a consequence of the flexible nature and interpenetrated configuration the activated **TIF-1** shows a relatively low BET surface area despite using $scCO_2$ for solvent exchange. Notably, the presence of both anionic nodes and cationic linkers in **TIF-1** may be leveraged for the selective small anion exchange or separation, an area that is currently being investigated and will be reported in due course.

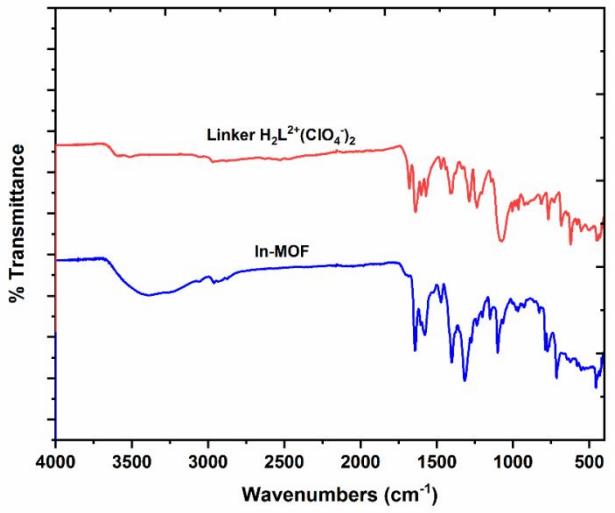

Fig. 4. ATR-IR spectroscopy of Linker $\mathbf{H_2L^{2+}(ClO_4^-)_2}$: ($cm^{-1}$) ν(amine C–H), 2967-2865; ν(COOH), 1679; ν(C=N), 1638; $\nu(ClO_4^-)$, 1072 and 621 and **TIF-1**: (cm^{-1}) $\nu(H_2O)$, 3385; ν(amine C–H), 2961-2871; ν(C=N), 1642; ν(COO), 1578, 1316; $\nu(NO_3^-)$, 1402.

EXPERIMENTAL SECTION

Materials and Methods

Chemicals used for ligand and **TIF-1** preparation i.e. Methyl-4 hydroxybenzoate, hexamethylenetetramine, 2,2-dimethyl-1,3-propanediamine, $In(NO_3)_3{\cdot}xH_2O$, $Cu(ClO_4)_2{\cdot}6H_2O$, trifluoroacetic acid (TFA), HNO_3, acetonitrile (CH_3CN) and N,N-dimethylformamide (DMF) were purchased from Aldrich and used as received unless otherwise noted. The deuterated solvent for NMR studies i.e $CDCl_3$ and d_6-DMSO were acquired from Aldrich and used as received. The common reagents and common solvents were acquired locally and used as received. All ^1H and ^{13}C NMR spectra were recorded on a Bruker Avance 400 MHz spectrometers at 25 °C with chemical shifts given in parts per million (ppm) using residual solvent peak at 7.26 ppm as reference in the case of $CDCl_3$ and 2.5 ppm as reference in the case of d_6-DMSO. ESI mass spectra of the compounds were recorded using JEOL GCMATE II GC-MS. Fourier transform infrared spectra (FTIR) were recorded on a Nicolet 8700 FTIR spectrometer equipped with an attenuated total reflection (ATR) stage. Powder XRD diffraction data of the synthesized material was collected on a Rigaku Smart Lab diffractometer with Cu Kα radiation source (λ = 1.54 Å) with a 0.01 2θ step width and a 3° min^{-1} scan speed over the 2θ range of 4–50° at room temperature. IS, RSI and RS2 values of 0.33, 12 and 20 were used, respectively. TGA-MS measurements were performed on a SETARAM Labsys-Evo coupled to a Hiden QGA-pro using synthetic air as the carrier gas (20% O_2 in Ar, 30 ml/min, 5 °C/min). High resolution X-Ray Photoelectron Spectroscopy (HR-XPS) measurements were performed in an analysis chamber (UHV – 210-10 Torr during analysis) using a Versaprobe III – PHI Instrument (PHI, USA). The sample was irradiated with a Focused X-Ray AlKα monochromated X-rays source (1486.6eV) using an X-Ray beam (size 200micron, 50W, 15kV). The outcoming photoelectrons are directed to a Spherical Capacitor Analyzer (SCA). The sample charging was compensated by a Dual Beam charge neutralization based on a combination of a traditional electron flood gun and a low energy argon ion beam.

Synthesis of $H_2L^{2+}(ClO_4^-)_2$:

The new dicopper Robson-type ligand $\mathbf{H_2L^{2+}(ClO_4^-)_2}$ was synthesized with slight modification to a previously reported procedure.[18] In a 20 ml vial, aldehyde (40 mg, 0.2 mmol) was dissolved in 6 ml hot ethanol. 100 mg $Cu(ClO_4^-)_2{\cdot}6H_2O$ (0.27mmol), 23 μl CH_3COOH (0.4 mmol) and 21 mg 2,2-dimethyl-1,3-propanediamine (0.2 mmol) in 4 ml ethanol were added to the aldehyde solution. After addition, the vial was sealed and heated to 65 °C for 3 days. Prism like dark green crystals were collected and dried. (Yield 0.147 g, 81 %). ATR IR (cm^{-1}): ν (amine C–H), 2967-2865; ν (COOH), 1679; ν (C=N), 1638; $\nu(ClO_4^-)$, 1072 and 621. MS (ESI): m/z 745 $[H_2L^{2+}ClO_4^-]$.

Synthesis of TIF-1:

27 mg ligand, 2 mg $In(NO_3)_3{\cdot}xH_2O$, DMF (3mL), CH_3CN (2mL) and HNO_3 (0.2mL, 2.7M in DMF) were added to a 20 mL vial and the vial was sealed and placed in an 80 °C oven for 5 d, green prism like crystals of **TIF-1** were collected and air dried, 72 % Yield. ATR IR (cm^{-1}): $\nu(H_2O)$, 3385; ν (amine C–H), 2961-2871; ν (C=N), 1642; ν(COO), 1578, 1316; $\nu(NO_3^-)$, 1402.

Conflicts of interest

"There are no conflicts to declare".

Acknowledgements

We thank Prof. Timur Islamoglu and Prof. Omar K. Farha, from Northwestern University, United States, for their kind scientific discussions. Dr. Sofia Lipstman and Dr. Natalia Fridman, are greatly thanked for their assistance in single crystal X-ray analysis. Funding by the Israel Science Foundation (grant # 1266/17) and the Binational Science Foundation (grant #2017639), is acknowledged. Author SP greatly appreciates the

support of the Lady Davis excellences fellowship. Author K.B.I. gratefully acknowledges support from the U.S. Department of Energy (DOE) Office of Science, Basic Energy Sciences Program for separation (DE-FG02-08ER15967). Author Z.C. gratefully acknowledges research support from the U.S. Department of Energy's Office of Energy Efficiency and Renewable Energy (EERE) under award no. DE-EE0008816.

Notes and references

1 (a) D. J. Tranchemontagne, J. L. Mendoza-Cortes, M. O'Keeffe and O. M. Yaghi, *Chem. Soc. Rev.*, 2009, **38**, 1257-1283. (b) S. Horike, S. Shimomura and S. Kitagawa, *Nat. Chem.*, 2009, **1**, 695-704. (c) G. Ferey, *Chem. Soc. Rev.*, 2008, **37**, 191-214. (d) Y. Zhang, X. Zhang, J. Lyu, K.-i. Otake, X. Wang, L. R. Redfern, C. D. Malliakas, Z. Li, T. Islamoglu, B. Wang and O. K. Farha, *J. Am. Chem. Soc.,* 2018, **140**, 11179-11183. (e) P. Deria, D. A. Gómez-Gualdrón, W. Bury, H. T. Schaef, T. C. Wang, P. K. Thallapally, A. A. Sarjeant, R. Q. Snurr, J. T. Hupp and O. K. Farha, *J. Am. Chem. Soc.,* 2015, **137**, 13183-13190. (f) Y. Yan, A. E. O'Connor, G. Kanthasamy, G. Atkinson, D. R. Allan, A. J. Blake and M. Schröder, *J. Am. Chem. Soc.,* 2018, **140**, 3952-3958. (g) X. Zhang, B. L. Frey, Y.-S. Chen and J. Zhang, *J. Am. Chem. Soc.,* 2018, **140**, 7710-7715. (h) D. Tanaka, K. Nakagawa, M. Higuchi, S. Horike, Y. Kubota, T. C. Kobayashi, M. Takata and S. Kitagawa, *Angew. Chem., Int. Ed.*, 2008, **47**, 3914-3918.

2 (a) H. Li, K. Wang, Y. Sun, C. T. Lollar, J. Li and H.-C. Zhou, *Mater. Today*, 2018, **21**, 108-121. (b) M. Eddaoudi, J. Kim, N. Rosi, D. Vodak, J. Wachter, M. O'Keeffe and O. M. Yaghi, *Science*, 2002, **295**, 469-472. (c) N. L. Rosi, J. Eckert, M. Eddaoudi, D. T. Vodak, J. Kim, M. O'Keeffe and O. M. Yaghi, *Science*, 2003, **300**, 1127-1130. (d) H. Furukawa, N. Ko, Y. B. Go, N. Aratani, S. B. Choi, E. Choi, A. O. Yazaydin, R. Q. Snurr, M. O'Keeffe, J. Kim and O. M. Yaghi, *Science*, 2010, **329**, 424-428. (e) D. Yuan, D. Zhao, D. Sun and H.-C. Zhou, *Angew. Chem., Int. Ed.*, 2010, **49**, 5357-5361, S5357/5351-S5357/5312. (f) D. Alezi, Y. Belmabkhout, M. Suyetin, P. M. Bhatt, L. J. Weselinski, V. Solovyeva, K. Adil, I. Spanopoulos, P. N. Trikalitis, A.-H. Emwas and M. Eddaoudi, *J. Am. Chem. Soc.*, 2015, **137**, 13308-13318. (g) D. Wu, P.-F. Zhang, G.-P. Yang, L. Hou, W.-Y. Zhang, Y.-F. Han, P. Liu and Y.-Y. Wang, *Coord. Chem. Rev.,* 2021, **434**, 213709.

3 (a) M. S. Shah, M. Tsapatsis and J. I. Siepmann, *Chem. Rev.*, 2017, **117**, 9755-9803. (b) M. S. Alivand, M. Shafiei-Alavijeh, N. H. M. H. Tehrani, E. Ghasemy, A. Rashidi and S. Fakhraie, *Microporous Mesoporous Mater.*, 2019, **279**, 153-164.

4 (a) J.-R. Li, J. Sculley and H.-C. Zhou, *Chem. Rev.*, 2012, **112**, 869-932. (b) J. Won, J. S. Seo, J. H. Kim, H. S. Kim, Y. S. Kang, S.-J. Kim, Y. Kim and J. Jegal, *Adv. Mater.*, 2005, **17**, 80-84. (c) S. Basu, A. Cano-Odena and I. F. J. Vankelecom, *J. Membr. Sci.*, 2010, **362**, 478-487. (d) E. V. Perez, K. J. Balkus, J. P. Ferraris and I. H. Musselman, *J. Membr. Sci.*, 2009, **328**, 165-173.

5 (a) J. An and N. L. Rosi, *J. Am. Chem. Soc.*, 2010, **132**, 5578-5579. (b) L. M. Rodriguez-Albelo, E. Lopez-Maya, S. Hamad, A. R. Ruiz-Salvador, S. Calero and J. A. R. Navarro, *Nat. Commun.*, 2017, **8**, 14457. (c) M. Plabst, L. B. McCusker and T. Bein, *J. Am. Chem. Soc.*, 2009, **131**, 18112-18118. (d) T. K. Maji, R. Matsuda and S. Kitagawa, *Nat. Mater.*, 2007, **6**, 142-148.

6 (a) L. Ma, J. M. Falkowski, C. Abney and W. Lin, *Nat. Chem.*, 2010, **2**, 838-846. (b) H. Jiang, W. Zhang, X. Kang, Z. Cao, X. Chen, Y. Liu and Y. Cui, *J. Am. Chem. Soc.*, 2020, **142**, 9642-9652. (c) J. Y. Lee, O. K. Farha, J. Roberts, K. A. Scheidt, S. B. T. Nguyen and J. T. Hupp, *Chem. Soc. Rev.*, 2009, **38**, 1450-1459. (d) X. Zhang, Z. Huang, M. Ferrandon, D. Yang, L. Robison, P. Li, T. C. Wang, M. Delferro and O. K. Farha, *Nat. Catal.*, 2018, **1**, 356-362. (e) L. Jiao and H.-L. Jiang, *Chem*, 2019, **5**, 786-804. (f) Y. Liu, W. Xuan and Y. Cui, *Adv. Mater.*, 2010, **22**, 4112-4135. (g) J. Liu, Y. Zhao, L.-L. Dang, G. Yang, L.-F. Ma, D.-S. Li and Y. Wang, *Chem. Commun.*, 2020, **56**, 8758-8761. (h) J. Liu, G.-P. Yang, J. Jin, D. Wu, L.-F. Ma and Y.-Y. Wang, *Chem. Commun.,* 2020, **56**, 2395-2398.

7 (a) C. Khoury, C. Gadipelly, S. Pappuru, D. Shpasser and O. M. Gazit, *Adv. Funct. Mater.,* 2020, **30**, 1901385. (b) L. Ma and W. Lin, *Angew. Chem., Int. Ed.*, 2009, **48**, 3637-3640, S3637/3631-S3637/3612. (c) D.-C. Zhong, L.-Q. Liao, J.-H. Deng, Q. Chen, P. Lian and X.-Z. Luo, *Chem. Commun.*, 2014, **50**, 15807-15810. (d) Y.-N. Gong, Y.-R. Xie, D.-C. Zhong, Z.-Y. Du and T.-B. Lu, *Cryst. Growth Des.,* 2015, **15**, 3119-3122.

8 (a) A. Schneemann, V. Bon, I. Schwedler, I. Senkovska, S. Kaskel and R. A. Fischer, *Chem. Soc. Rev.*, 2014, **43**, 6062-6096. (b) A. U. Ortiz, A. Boutin, A. H. Fuchs and F.-X. Coudert, *Phys. Rev. Lett.*, 2012, **109**, 195502/195501-195502/195505. (c) Z.-J. Lin, J. Lu, M. Hong and R. Cao, *Chem. Soc. Rev.*, 2014, **43**, 5867-5895. (d) O. M. Yaghi, *Nat. Mater.*, 2007, **6**, 92-93.

9 (a) H.-L. Jiang, T. A. Makal and H.-C. Zhou, *Coord. Chem. Rev.*, 2013, **257**, 2232-2249. (b) Y.-N. Gong, D.-C. Zhong and T.-B. Lu, *CrystEngComm*, 2016, **18**, 2596-2606. (c) M. Vicent-Morales, I. J. Vitorica-Yrezabal, M. Souto and G. Minguez Espallargas, *CrystEngComm*, 2019, **21**, 3031-3035.

10 (a) J. Zhang, L. Wojtas, R. W. Larsen, M. Eddaoudi and M. J. Zaworotko, *J. Am. Chem. Soc.*, 2009, **131**, 17040-17041. (b) S. Bureekaew, H. Sato, R. Matsuda, Y. Kubota, R. Hirose, J. Kim, K. Kato, M. Takata and S. Kitagawa, *Angew. Chem., Int. Ed.*, 2010, **49**, 7660-7664, S7660/7661-S7660/7613. (c) J.-U. Duan, J.-G. Bai, B.-S. Zheng, Y.-Z. Li and W.-C. Ren, *Chem. Commun.*, 2011, **47**, 2556-2558. (d) S. Surinwong, N. Yoshinari, T. Kojima and T. Konno, *Chem. Commun.*, 2016, **52**, 12893-12896. (e) O. K. Farha, C. D. Malliakas, M. G. Kanatzidis and J. T. Hupp, *J. Am. Chem. Soc.*, 2010, **132**, 950-952.

11 (a) M. Dan-Hardi, H. Chevreau, T. Devic, P. Horcajada, G. Maurin, G. Ferey, D. Popov, C. Riekel, S. Wuttke, J.-C. Lavalley, A. Vimont, T. Boudewijns, D. de Vos and C. Serre, *Chem. Mater.*, 2012, **24**, 2486-2492. (b) M. O'Keeffe, M. A. Peskov, S. J. Ramsden and O. M. Yaghi, *Acc. Chem. Res.*, 2008, **41**, 1782-1789. (c) J.-M. Gu, S.-J. Kim, Y. Kim and S. Huh, *CrystEngComm*, 2012, **14**, 1819-1824.

12 D. Sun, Z.-H. Yan, M. Liu, H. Xie, S. Yuan, H. Lu, S. Feng and D. Sun, *Cryst. Growth Des.*, 2012, **12**, 2902-2907.

13 (a) Y. Yuan, J. Li, X. Sun, G. Li, Y. Liu, G. Verma and S. Ma, *Chem. Mater.*, 2019, **31**, 1084-1091. (b) D. Reinares-Fisac, L. M. Aguirre-Diaz, M. Iglesias, N. Snejko, E. Gutierrez-Puebla, M. A. Monge and F. Gandara, *J. Am. Chem. Soc.*, 2016, **138**, 9089-9092.

14 L. M. Aguirre-Diaz, D. Reinares-Fisac, M. Iglesias, E. Gutierrez-Puebla, F. Gandara, N. Snejko and M. A. Monge, *Coord. Chem. Rev.*, 2017, **335**, 1-27.

15 J.-H. Liu, Y.-J. Qi, D. Zhao, H.-H. Li and S.-T. Zheng, *Inorg. Chem.*, 2019, **58**, 516-523.

16 (a) N. H. Pilkington and R. Robson, *Aust. J. Chem.*, 1970, **23**, 2225-2236. (b) A. J. Atkins, D. Black, A. J. Blake, A. Marin-Becerra, S. Parsons, L. Ruiz-Ramirez and M. Schroder, *Chem. Commun.*, 1996, 457-464.

17 (a) M. Swadzba-Kwasny, L. Chancelier, S. Ng, H. G. Manyar, C. Hardacre and P. Nockemann, *Dalton Trans.*, 2012, **41**, 219-227. (b) C. E. Nanayakkara, P. M. Jayaweera, G. Rubasinghege, J. Baltrusaitis and V. H. Grassian, *J. Phys. Chem. A*, 2014, **118**, 158-166.

18 M. Zhou, Z. Ju and D. Yuan, *Chem. Commun.*, 2018, **54**, 2998-3001.

19 B.-Q. Song, X.-L. Wang, Y.-T. Zhang, X.-S. Wu, H.-S. Liu, K.-Z. Shao and Z.-M. Su, *Chem. Commun.*, 2015, **51**, 9515-9518.

20 S. Hazra, S. Bhattacharya, M. K. Singh, L. Carrella, E.

Rentschler, T. Weyhermueller, G. Rajaraman and S. Mohanta, *Inorg. Chem.*, 2013, **52**, 12881-12892.